Water Adsorption in Metal–Organic Frameworks with Open-Metal Sites

Xuan Peng
Dept. of Automation, College of Information Science and Technology, Beijing University of Chemical Technology, Beijing 100029, China

Dept. of Chemical and Biomolecular Engineering, University of California, Berkeley, CA 94720

Li-Chiang Lin
Dept. of Chemical and Biomolecular Engineering, University of California, Berkeley, CA 94720

Weizhen Sun
Dept. of Chemical and Biomolecular Engineering, University of California, Berkeley, CA 94720

State-Key Laboratory of Chemical Engineering, East China University of Science and Technology, Shanghai 200237, China

Key Laboratory of Advanced Control and Optimization for Chemical Processes, East China University of Science and Technology, Shanghai 200237, China

Berend Smit
Dept. of Chemical and Biomolecular Engineering, University of California, Berkeley, CA 94720

Dept. of Chemistry, University of California, Berkeley CA 94720

Materials Sciences Division, Lawrence Berkeley National Laboratory, Berkeley, CA 94720

DOI 10.1002/aic.14707
Published online December 17, 2014 in Wiley Online Library (wileyonlinelibrary.com)

H_2O adsorptions inside porous materials, including silica zeolites, zeolite imidazolate frameworks, and metal–organic frameworks (MOFs) using molecular simulations with different water models are investigated. Due to the existence of coordinately unsaturated metal sites, the predicted adsorption properties in M-MOF-74 (M = Mg, Ni, Co, Zn) and Cu-BTC are found to be greatly sensitive to the adopted H_2O models. Surprisingly, the analysis of the orientations of H_2O minimum energy configuration in these materials show that three-site H_2O models predict an unusual perpendicular angle of H_2O plane with respect to the Metal-O_4 plane, whereas those models with more than three sites give a more parallel angle that is in better agreement with the one obtained from density functional theory (DFT) calculations. In addition, the use of these commonly used models estimates the binding energies with the values lower than the ones computed by DFT ranging from 15 to 40%. To correct adsorption energies, simple approach to adjust metal-O(H_2O) sigma parameters to reproduce the DFT-calculated binding energies is used. With the refined parameters, the computed water isotherms inside Mg-MOF-74 and Cu-BTC are in reasonable agreement with experimental data, and provide significant improvement compared to the predictions made by the original models. Further, a detailed inspection on the water configurations at higher-pressure region was also made, and observed that there is an interesting two-layer water network formed using three- and four-site models. © 2014 American Institute of Chemical Engineers *AIChE J*, 61: 677–687, 2015

Keywords: adsorption, molecular simulation, water, metal, organic frameworks

Introduction

Carbon capture and sequestration (CCS), a process of capturing carbon dioxide emitted from burning fossil fuel and sequestrating it in the underground, is a potential means to mitigate global warming and ocean acidification.[1] Advanced technologies based on regenerative capture are therefore required. Adsorption via porous materials to remove CO_2 from flue gas has been of great interests for its economic

Additional Supporting Information may be found in the online version of this article.

Xuan Peng and Li-Chiang Lin contributed equally to the work.

Correspondence concerning this article should be addressed to B. Smit at Berend-Smit@berkeley.

Table 1. Force-Field Parameters and Geometries of Considered H_2O Models in This Study

Model	σ (Å)	ε (K)	l_1 (Å)	l_2 (Å)	q_1 (e)	q_2 (e)	θ (°)	φ (°)
SPC	3.1656	78.20	1.0000	–	+0.410	−0.8200	109.47	–
SPC/E	3.1656	78.20	1.0000	–	+0.4238	−0.8476	109.47	–
TIP3P	3.1506	76.54	0.957	–	+0.4170	−0.8340	104.52	–
TIP4P	3.154	78.02	0.957	0.15	+0.5200	−1.0400	104.52	52.26
TIP4P-Ew	3.1643	81.90	0.957	0.125	+0.5242	−1.0484	104.52	52.26
TIP5P	3.12	80.51	0.957	0.70	+0.2410	−0.2410	104.52	109.47
TIP5P-Ew	3.097	89.574	0.957	0.70	+0.2410	−0.2410	104.52	109.47
TIP6P	3.115_{OO}	85.9766_{OO}	0.980	0.889_{L}	+0.477	-0.044_{L}	108.00	111.00
	0.673_{HH}	13.8817_{HH}		0.230_{M}		-0.866_{M}		

The definition of these geometrical parameters shown in this table can be found in Figure 1.

and environmental advantages.[2] A key to implement adsorption technology in a large-scale commercial application is to seek a potential adsorbent that exhibits a lower parasitic energy (i.e., the electric load diverted from a power plant) compared to the near-term technology, amine scrubbing. In one of our recent works,[3] Lin et al. screened hundreds of thousands of zeolites and zeolitic imidazolate framework (ZIF)[4–6] structures, and identified many different structures that have the potential to reduce the parasitic energy of CCS by 30–40%. Furthermore, metal–organic frameworks (MOFs),[7–9] a relatively new class of porous materials, consist of metal ions or clusters and organic linkers. Their chemical functionalities and pore structures can be controllably tailored by assembling a variety of organic linker and metal oxide. This highly tunable characteristic also makes them as one of the most promising candidates for CCS application.

The considered flue gas in most of the adsorption studies for CCS is usually simplified as a binary gas mixture composed of CO_2 and N_2 while other flue gas components (e.g., H_2O, SO_x, NO_x) are neglected. As is well known, flue gas can contain up to about 10% molar concentration of water.[3] Water adsorption in porous materials is therefore of great importance, in particular as water may compete for the same adsorption sites. In addition, the adsorption of water is interesting from a scientific point of view as, unlike CO_2, water can form hydrogen bonds and understanding the role of these hydrogen bonds is important in the adsorption behavior. For example, Lin et al. showed that the presence of H_2O preferentially occupies the CO_2 binding sites, resulting in a large reduction of the CO_2 uptake.[10] In contrast, a computational and experimental study by Yazaydin et al.[11] demonstrated that the adsorption behavior of CO_2 in Cu-BTC could be tuned by the presence of water molecules coordinated to open-metal sites. The interaction between the quadruple moment of CO_2 and the electric field created by water molecules leads to enhanced CO_2 uptake and its selectivity over N_2 and CH_4. Greathouse and Allendorf[12] found that the structure of IRMOF-1 deforms when the framework interacts with certain amount of water, which is attributed to the replacement of oxygen atoms of MOF with the ones of water in the Zn coordination shells. Additionally, water confined in carbon nanotubes with a critical diameter can undergo a phase transition into an ice-like state[13,14]; a nonpolar carbon nanotube can be spontaneously filled by a one-dimensionally ordered and continuously chain of water molecules, and this pulse-like transmission of water molecules through the nanotube results from a tight hydrogen-bonding network inside the tube.[15]

In this study, molecular simulations are conducted to explore water adsorption properties adsorbed inside varying porous materials, including silicate zeolites, zeolitic imidazole frameworks (ZIFs), and MOFs. It should be noted that a comprehensive understanding of water phase is still inadequate. As a consequence, at least 46 distinct molecular water models have been proposed[16] for reproducing few specific properties of water. In this work, we used a variety of H_2O models to offer insights into the adsorption behavior of water in different porous materials. Several important adsorption properties including binding energies, heats of adsorption, isotherms, and spatial orientations and density profiles of water configurations are investigated. Furthermore, a simple strategy was used to correct force field based on the binding energies computed by density functional theory (DFT) calculations. Comparisons of adsorption isotherms with the available experimental data are also made, justifying the effectiveness of the force field obtained in this study.

Molecular Simulation

Grand-canonical Monte Carlo (GCMC)[17] and canonical Monte Carlo simulations with gradual decrease in temperature are performed to compute the adsorption isotherms and binding geometry/energy, respectively. In these simulations, the frameworks are treated as rigid and periodic boundary conditions are applied. Nonelectrostatic pair-wise potential is truncated and shifted to zero at a cutoff radius of 12.8 Å, a value that is sufficiently large and has been widely used in most simulation studies reported in the literature. Ewald summation technique is used to compute the long-range electrostatic interaction. The simulation box is composed of multiple unit cells to ensure each perpendicular dimension at least twice of cutoff radius. To accelerate the simulations, three-dimensional tabular table of interactions between H_2O and frameworks with grid spacing of 0.15 Å are precalculated, and cubic-spline interpolation is adopted. In addition, to obtain accurate ensemble averages in GCMC simulations, at least millions of configurations generated by random translation, rotation, regrowth, and swap moves are sampled in each simulation.

The geometrical and force-field parameters of the implemented H_2O models[18–26] are provided in Table 1, and the definition of these geometrical parameters can be found in Figure 1. For pure-silica zeolite MFI, we use the force field proposed by Castillo et al.[18] while the UFF force field[27] is adopted for ZIF-8 and other MOF materials. The Lorentz–Berthelot combining rule is used to determine the cross interaction parameters. A more detailed information of the material structures can be found in Refs. 3,18,28–32.

We studied 11 structures selected from various classes of materials. For IRMOF-1,[8,9] ZIF-8,[4,5] MOF-177,[33,34] Cu-

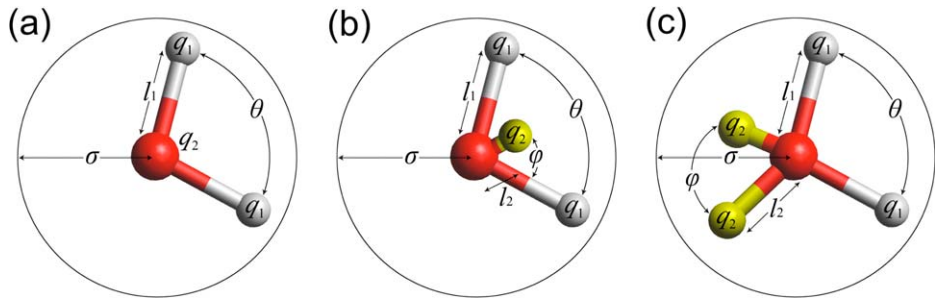

Figure 1. Definitions of adopted water models: (a) three-sites (SPC, SPC/E and TIP3P), (b) four-sites (TIP4P and TIP4P-Ew), and (c) five-sites (TIP5P and TIP5P-Ew).

The six-site (TIP6P) model is similar to that of five-site model with two long-pair sites M but has one extra site M along the bisector between two OH bonds similar to the four-site model. The atomic charges of pseudosites M and L in the six-site model have values of $q_{2,M}$ and $q_{2,L}$, respectively. [Color figure can be viewed in the online issue, which is available at wileyonlinelibrary.com.]

BTC,[7] Co-MOF-74,[35] and Ni-MOF-74,[36] the atomic charges of framework atoms come from Yazaydin et al.[37] while for MIL-47[38,39] and UMCM-1,[40] charges are taken from our previous works.[29,31] For Mg-MOF-74[41–44] and Zn-MOF-74,[45,46] we perform simulations with two different sets of framework coordinates and corresponding charges. First set uses the DFT-optimized structures with atomic charges fitted from REPEAT scheme as obtained from our previous work.[32,47] Another set uses the experimental structures and the charges from Yazaydin et al.[37]

To analyze the microstructure of H_2O adsorbed in porous materials, probability densities of oxygen atoms of H_2O molecules are computed.[48] These calculation involve dividing the unit cell of the framework into small elements along z-direction in Cartesian coordinates and the x,y directions in radial-, angular-directions in cylindrical coordinate (see Supporting Information Figure S1a), and the average number of the oxygen atoms residing in each element during simulation is computed. Note that these values are properly normalized to make the summation of probabilities to unity.

In addition to probability densities, two orientational order parameters are calculated. The orientational order parameter[49] as a function of distance, r, from center of the pore along z axis (i.e., pore axis) with respect to the Mg-MOF-74 surface is defined as

$$S(r)=\left\langle \frac{3}{2}\cos^2\alpha-\frac{1}{2}\right\rangle \tag{1}$$

where α is the angle between the normal vector to the plane of an H_2O molecule and the normal vector to the Mg-MOF-74 surface. The bracket denotes an average over all of the sampled molecules within a distance of r and $r+dr$. For Mg-MOF-74 that has cylindrical pores along the z axis, the normal vector $\vec{n}$ to the Mg-MOF-74 surface at the position of a given H_2O molecule is calculated from the coordinates of the center of mass of the H_2O molecule (x_0, y_0)

$$\vec{n}=-x_0/(x_0^2+y_0^2)^{1/2}\hat{x}-y_0/(x_0^2+y_0^2)^{1/2}\hat{y}$$

where $\hat{x}$ and $\hat{y}$ are unit vectors along the x- and y-directions, respectively (see Supporting Information Figure S2b). $S\sim -0.5$ and ~ 1 indicate that H_2O molecules are perpendicular and parallel to the Mg-MOF-74 surface, respectively; whereas $S\sim 0$ reveals no particular orientation with respect to the surface.

Similarly, the orientational order parameter with respect to the pore axis is given by

$$S_z(r)=\left\langle \frac{3}{2}\cos^2\beta-\frac{1}{2}\right\rangle \tag{2}$$

where β is the angle between the normal vector to the plane of an H_2O molecule and the pore axis. Similarly, $S_z\sim -0.5$ and ~ 1 indicates that H_2O molecules perpendicular and parallel to the pore axis, respectively, whereas $S_z\sim 0$ reveals no particular orientation with respect to the pore axis.

Results and Discussion

Adsorption properties at infinite dilution condition

Henry coefficients and isosteric heats at zero coverage were calculated for 11 structures selected from various classes of materials at 298 K (see Table 2; data at 318 K can be found in Supporting Information Table S1).

The results at 298 K show that ZIF-8, IRMOF-1, and UMCM-1 have the smallest Henry coefficients ($\sim 10^{-6}$ mol/kg/Pa) and heats of adsorption ($\sim$10 kJ/mol) while the zeolite MFI has an order of magnitude higher in Henry coefficients (i.e., $\sim 10^{-5}$ mol/kg/Pa). For Cu-BTC and MOF-74 series, the Henry coefficients and heats of adsorption are the largest among these MOFs, which can be attributed to the existences of these open-metal sites.

More importantly, we observe that the details of the H_2O models play an important role in the adsorption properties.

Table 2. H_2O Adsorption Properties Inside Different Materials at 298 K and Infinite Dilution Condition

	Henry Coefficient (mol/kg/Pa)		Isosteric Heats of Adsorption (kJ/mol)	
Material	SPC/E	TIP5P-Ew	SPC/E	TIP5P-Ew
MFI	2.87 E −05	2.39 E −05	−26.61	−26.33
ZIF-8	2.31 E −06	2.25 E −06	−11.18	−10.36
IRMOF-1	3.25 E −06	3.01 E −06	−10.49	−9.47
UMCM-1	4.83 E −06	5.12 E −06	−10.80	−11.62
MOF-177	3.85 E −03	5.00 E −03	−55.32	−56.71
MIL-47	1.99 E −04	4.39 E −04	−33.49	−34.91
Cu-BTC	1.87 E −04	8.96 E −04	−31.69	−39.79
Co-MOF-74	2.46 E −02	1.96 E −01	−47.98	−56.70
Ni-MOF-74	1.12 E −03	6.88 E −03	−40.05	−48.39
Mg-MOF-74[a]	8.55 E −03	4.97 E −02	−43.81	−50.88
Mg-MOF-74[b]	1.87 E −03	8.01 E −03	−39.93	−45.96
Zn-MOF-74[a]	1.83 E −04	6.77 E −04	−33.35	−39.59
Zn-MOF-74[b]	2.53 E −02	1.13 E −01	−47.00	−52.47

[a]Atomic charges are adopted from our previous works for Zn-MOF-74[32] and Mg-MOF-74,[47] respectively.
[b]Atomic charges are adopted from Yazaydin et al.[37]

Table 3. H_2O Orientation of Minimum Energy Configuration in Mg-MOF-74[a] and Cu-BTC[b]

Model	Distance Between Mg—O(H_2O)[a] (Å)	Angle Between H_2O Plane and MgO_4 Plane[a] (°)	Distance Between Cu—O(H_2O)[b] (Å)	Angle Between H_2O Plane and CuO_4 Plane[b] (°)
SPC	2.496	89.77	2.379	89.95
SPC/E	2.487	89.85	2.372	89.41
TIP3P	2.490	78.87	2.369	89.70
TIP4P	2.507	20.51	2.433	36.26
TIP4P-Ew	2.507	19.36	2.427	27.79
TIP5P	2.408	31.96	2.305	24.74
TIP5P-Ew	2.407	32.11	2.306	25.55
TIP6P	2.468	11.49	2.382	11.73

[a]Atomic charges are adopted from our previous work.[47]
[b]Atomic charges are adopted from Yazaydin et al.[37]

For MFI, ZIF-8, IRMOF-1, UMCM-1, and MOF-177, both SPC/E and TIP5P-Ew models have almost identical adsorption properties. For the adsorption in those MOFs with open-metal sites, however, we observe large differences in adsorption for the different H_2O models. The computed Henry coefficients and heats of adsorption with TIP5P-Ew model are larger than those of SPC/E model by ~1 order of magnitude and ~10%, respectively. In addition, the adsorption properties are also sensitive to the partial atomic charges, compared with the results obtained from REPEAT charges with those obtained ChelpG charges (as used by Yazaydin et al.).

Binding orientations and energies

As open-metal sites MOFs exhibit unique adsorption affinities compared to other materials, we focus on Cu-BTC and Mg-MOF-74 as two typical representatives for these materials. Although the UFF force field has been shown to yield poor estimates of CO_2 adsorption isotherms in these materials, in particular Mg-MOF-74,[32] it is still instructive to use UFF to investigate the effect of the water models on the adsorption properties. In Table 3, we list the computed metal-O(H_2O) distance and spatial orientations of the H_2O binding configuration in Mg-MOF-74 and Cu-BTC.

Table 3 shows the distances between Mg atom and O(H_2O) of binding configurations approximate 2.49, 2.51, 2.41, and 2.47 Å for three-site models (SPC, SPC/E, and TIP3P), four-site models (TIP4P and TIP4P-Ew), five-site models (TIP5P and TIP5P-Ew), and six-site model (TIP6P), respectively. Although the Mg—O distances of various models are similar, the angles between H_2O plane and MgO_4 plane reveal a remarkable difference. Interestingly, a clear transition from the perpendicular orientation (~90°, for three-site models) to the parallel orientation (<35°, for four-site, five-site, and six-site models) is found. Similar behavior has also been seen for H_2O adsorbing in Cu-BTC.

To obtain some insights which of these water models give a correct description, we compare the obtained geometries with the ones computed by quantum mechanical calculations. The binding geometry of H_2O in Mg-MOF-74 obtained from DFT calculations with the implementation of a nonlocal van der Waals density functional, vdW-DF2,[50] for dispersion interactions shows that the distance of Mg—O is 2.256 Å and the angle between H_2O plane and MgO_4 plane is 36.29° (Lin et al. unpublished). For Cu-BTC, the DFT-PW91-GGA results from Watanabe and Sholl[51] show a Cu—O distance of 2.304 Å and the corresponding angle of 48.6°. Another DFT-CC calculation from Grajciar et al.[52] shows that the Cu—O distance is 2.19 Å, close to the experimental value of 2.17 Å. From these data, we can see that the water models with more than three sites provide a better quantitative agreement of the binding orientations with the DFT results. Note that five-site models have the best agreement with the DFT results among these models.

Table 4 further summarizes the H_2O binding energies computed by different water models in Mg-MOF-74 and Cu-BTC, which have values ranging from −47 to −60 and −36 to −47 kJ/mol, respectively. A detailed decomposition of energies indicates that the electrostatic contribution dominates the total energies. As a comparison, the binding energies calculated from DFT calculations are −69.85 kJ/mol for Mg-MOF-74 (Lin et al. unpublished) and −55.3 kJ/mol for Cu-BTC.[52] Clearly, the energies from classical UFF deviate at least 15% from DFT results for all H_2O models. Among these models, in particular, five-site models show a better agreement with the DFT result, which is consistent to the aforementioned orientation analysis.

Table 4. Binding Energy of H_2O Adsorbed in Mg-MOF-74[a] and Cu-BTC[b]

		Host-Adsorbate[a] (kJ/mol)			Host-Adsorbate[b] (kJ/mol)	
Model	Total[a] (kJ/mol)	VDW	Coulomb	Total[b] (kJ/mol)	VDW	Coulomb
SPC	−48.43	3.12	−51.55	−36.41	6.14	−42.52
SPC/E	−50.18	3.54	−53.72	−37.86	6.64	−44.46
TIP3P	−48.65	1.21	−49.87	−36.77	6.35	−43.08
TIP4P	−47.16	6.57	−53.70	−37.28	10.25	−47.49
TIP4P-Ew	−48.55	5.52	−54.03	−37.67	9.29	−46.92
TIP5P	−59.55	8.14	−67.68	−47.51	12.28	−59.75
TIP5P-Ew	−60.17	7.56	−67.72	−47.65	11.90	−59.52
TIP6P	−50.25	4.26	−54.49	−38.63	8.13	−46.73

[a]Atomic charges are adopted from our previous work.[47]
[b]Atomic charges are adopted from Yazaydin et al.[37]

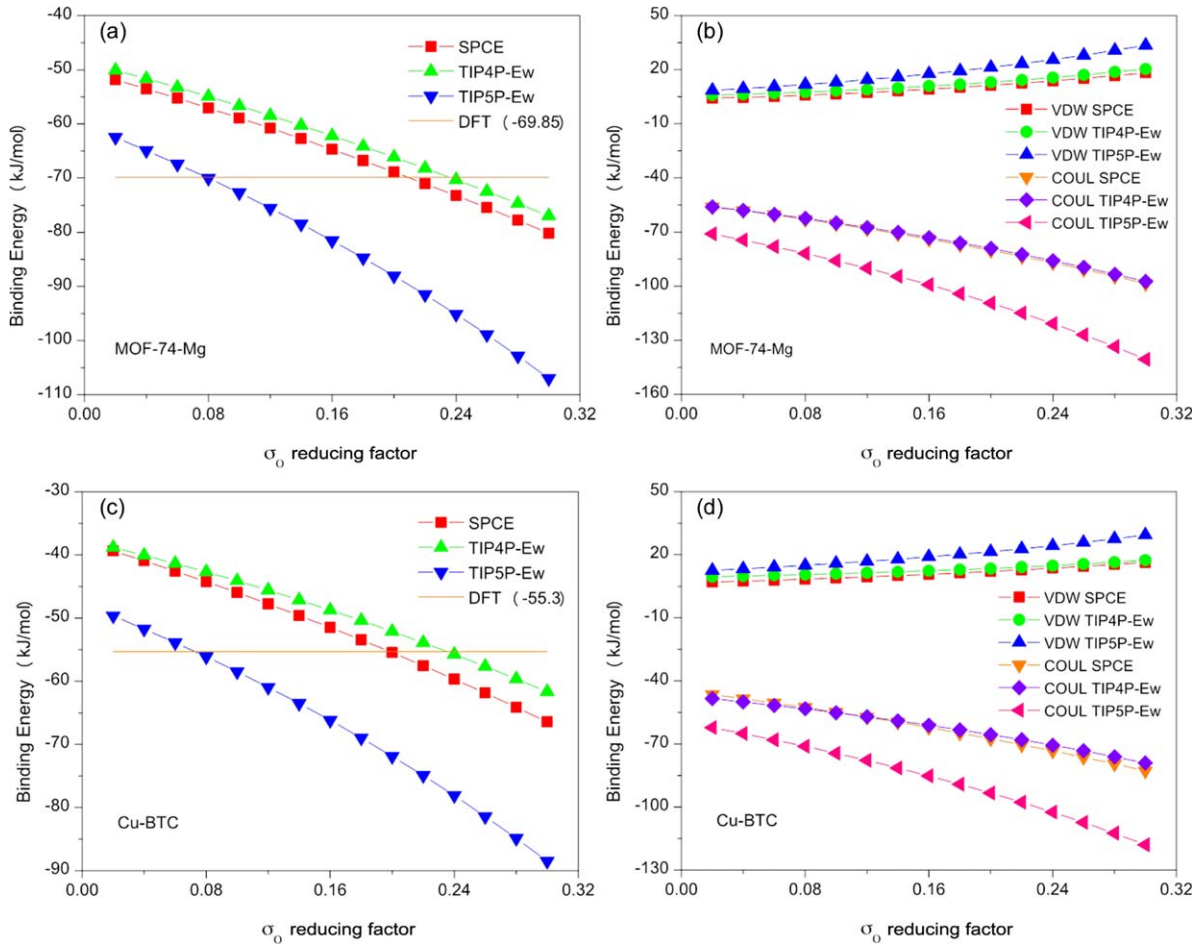

Figure 2. Binding energy and decomposed contribution of H_2O in (a, b) Mg-MOF-74 and (c, d) Cu-BTC as a function of reducing factor applied to the sigma parameter between Mg and O(H_2O).

[Color figure can be viewed in the online issue, which is available at wileyonlinelibrary.com.]

Force-field refinement

To improve the description of interactions between H_2O and open-site MOFs for those commonly used force fields, we use a simple refinement strategy in this study. Consistent with the work of Dzubak et al.,[32] we found that in UFF the repulsion between guest molecules and framework atoms, especially the metal centers, are too strong. To correct this, we decrease the crossing interaction parameter σ between O(H_2O) and metal centers by applying a reducing factor on the UFF parameters to effectively reduce the repulsion energy. As an example, a reducing factor of 0.1 indicates that the adjusted parameter has a value that is 90% of the original one. Note that this correction has also been used in one of the recent studies to predict the adsorptions of several small molecules in open metal-site materials.[53]

We apply these corrections to the SPC/E, TIP4P-Ew, and TIP5P-Ew water models. The total energies as well as detailed contributions as a function of reducing factor is shown in Figure 2; the total energies become more negative with increasing ratio. For both materials, the best fits to the

Table 5. H_2O Orientation of Minimum Energy Configuration in Mg-MOF-74[a] and Cu-BTC[b] with Refined Force-Field Parameter at Different Reducing Factor, σ_O

Model	σ_O Reducing Factor	Energy[a] (kJ/mol)	Distance Between Mg—O[a] (Å)	Angle Between H_2O Plane and MgO_4 Plane[a] (°)	Energy[b] (kJ/mol)	Distance Between Cu—O[b] (Å)	Angle Between H_2O Plane and CuO_4 Plane[b] (°)
SPC/E	0.18	−66.77	2.222	86.77	−53.45	2.123	89.98
	0.2	−68.87	2.193	86.61	−55.46	2.096	89.72
	0.22	−71.02	2.165	86.82	−57.54	2.07	89.98
TIP4P-Ew	0.22	−68.18	2.175	9.43	−53.90	2.097	4.67
	0.24	−70.29	2.146	9.13	−55.75	2.07	6.48
	0.26	−72.46	2.118	8.96	−57.66	2.044	7.97
TIP5P-Ew	0.06	−67.41	2.316	32.47	−53.88	2.22	27.59
	0.08	−70.01	2.285	32.65	−56.13	2.192	28.13
	0.1	−72.72	2.255	32.86	−58.49	2.163	28.76

[a]Atomic charges are adopted from our previous work.[47]
[b]Atomic charges are adopted from Yazaydin et al.[37]

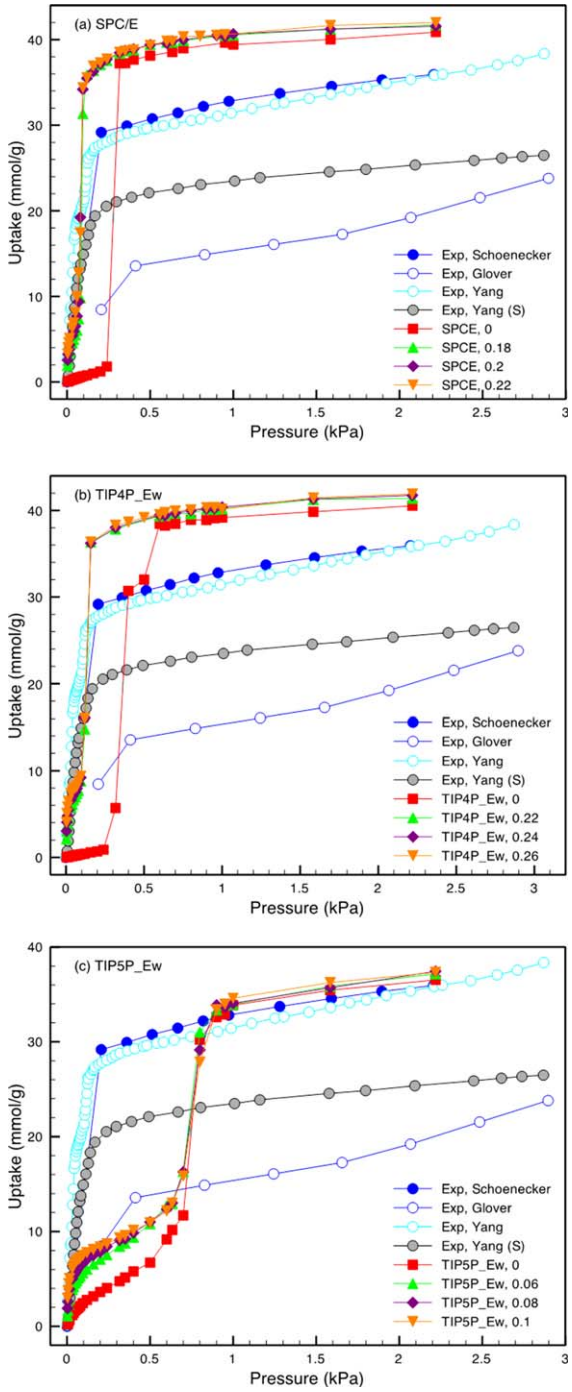

Figure 3. Comparison of the experimental H_2O isotherms in Mg-MOF-74 at 298 K with the simulated isotherms by both original and refined potentials with the use of (a) SPC/E, (b) TIP4P-Ew, and (c) TIP5P-Ew model.

The values of applied reducing factor are denoted in the legend. [Color figure can be viewed in the online issue, which is available at wileyonlinelibrary.com.]

DFT-computed binding energies are obtained at the reducing factors, σ, of 0.2, 0.26, and 0.08 for SPC/E, TIP4P-Ew, and TIP5P-Ew, respectively. Table 5 further gives the H_2O orientations calculated from our refined force-field parameters. Compared to the ones given in Table 3, it shows that the refinements do not substantially change the binding orientations although the refined TIP4P-Ew model has a smaller angle than the one without refinement (i.e., ~20 to ~10° in Mg-MOF-74). It should be noted that the binding distances computed by these refined models are much closer to the DFT results.

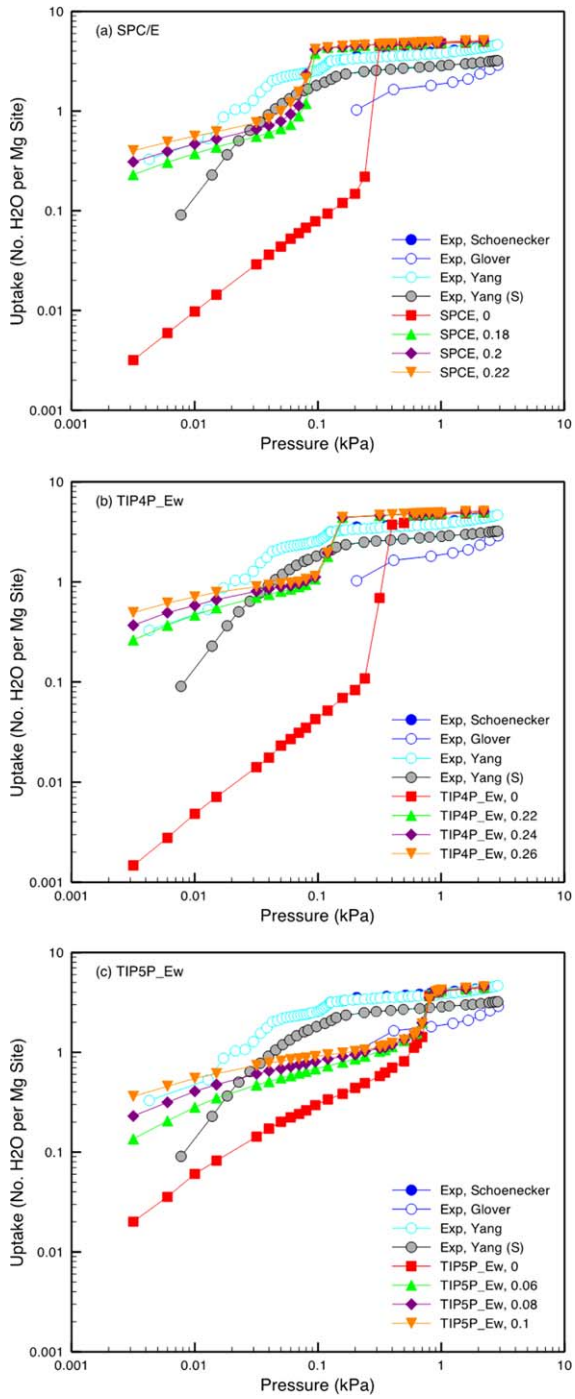

Figure 4. (log–log scale) Comparison of experimental H_2O isotherms in Mg-MOF-74 at 298 K with the simulated isotherms by both original and refined potentials with the use of (a) SPC/E, (b) TIP4P-Ew, and (c) TIP5P-Ew model.

The units in uptake are the number of H_2O molecules per metal site. The values of applied reducing factor are denoted in the legend. [Color figure can be viewed in the online issue, which is available at wileyonlinelibrary.com.]

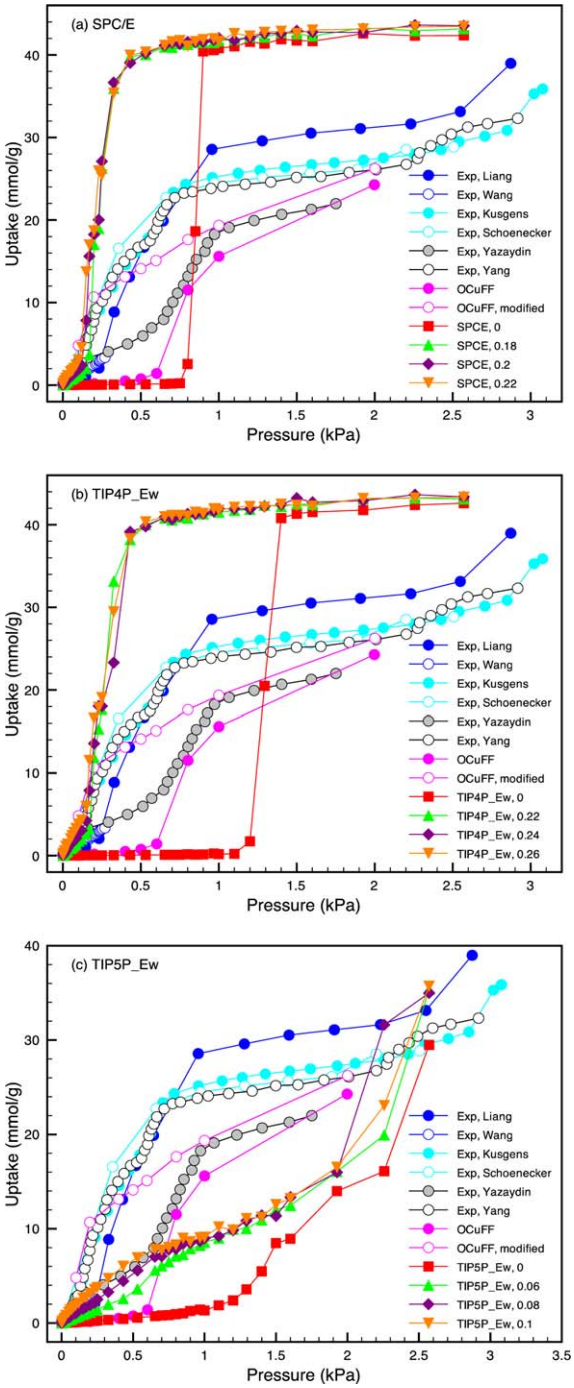

Figure 5. Comparison of the experimental H_2O isotherms in Cu-BTC at 298 K with the simulated isotherms by both original and refined potentials with the use of (a) SPC/E, (b) TIP4P-Ew, and (c) TIP5P-Ew model, and the OCuFF potential proposed by Zang et al.[57]

The values of applied reducing factor are denoted in the legend. [Color figure can be viewed in the online issue, which is available at wileyonlinelibrary.com.]

Adsorption isotherms

In Figures 3 and 4, we compare the GCMC-computed adsorption isotherms with the experimental ones for Mg-MOF-74. Clearly, we can see that the predicted uptake by these refined potentials is in good agreement with the experimental data at low-pressure region, and provide significant improvements compared to those without any refinements. Additionally, the occurrence of capillary condensation

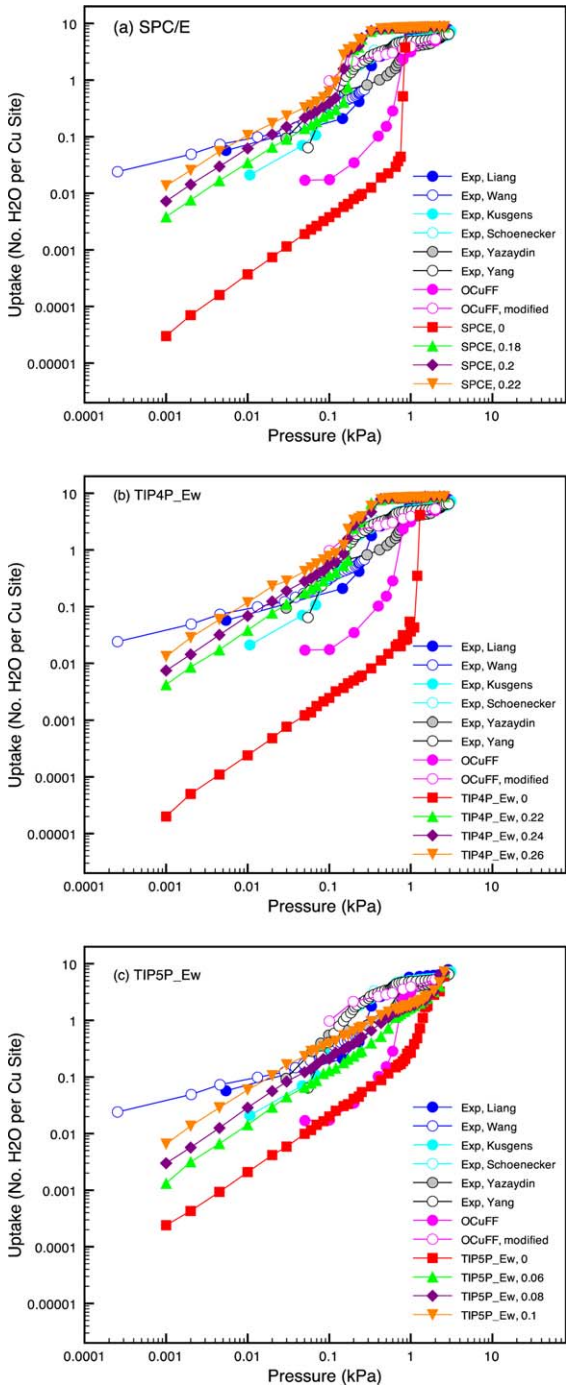

Figure 6. (log–log scale) Comparison of the experimental H_2O isotherms in Cu-BTC at 298 K to the simulated isotherms by both original and refined potentials with the use of (a) SPC/E, (b) TIP4P-Ew, and (c) TIP5P-Ew model, and the OCuFF potential proposed by Zang et al.[57]

The units in uptake are the number of H_2O molecules per metal site. The values of applied reducing factor are denoted in the legend. [Color figure can be viewed in the online issue, which is available at wileyonlinelibrary.com.]

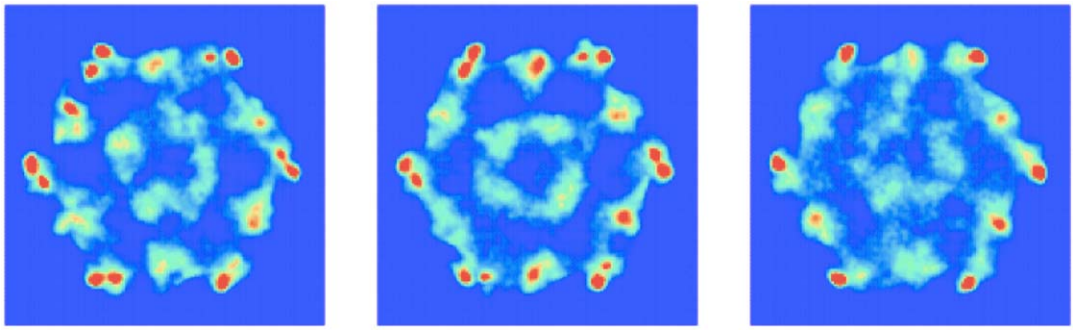

Figure 7. Density maps of oxygen atoms of H_2O molecules in Mg-MOF-74 at 2.2 kPa and 298 K with the views along *z* axis with the use of (a) SPC/E, (b) TIP4P-Ew, and (c) TIP5P-Ew models.

Warmer colors represent higher probabilities of finding oxygen atom of H_2O molecule. [Color figure can be viewed in the online issue, which is available at wileyonlinelibrary.com.]

of these models is at uptake of ~1 H_2O per Mg site with the refined force field, which is expected given that the Mg—H_2O interaction is sufficiently strong and one would anticipate that H_2O molecules tend to occupy all available metal sites first (i.e., H_2O per Mg site). In contrast, for SPC/E and TIP4P-Ew model, the original force-field models predict the transition at a loading of 0.1 mol/kg. Interestingly, TIP5P-Ew model shows a very different behavior in the adsorption mechanism compared to that of SPC/E and TIP4P-Ew. The predicted isotherm by TIP5P-Ew has a pronounced plateau, before capillary condensation sets in. This plateau is not observed in experimental data.

At the higher-pressure region (i.e., >1 kPa), the predicted uptakes by SPC/E and TIP4P-Ew models are higher than the experimental values, whereas the TIP5P-Ew model estimates lower uptake but agrees well with the Schoenecker's work.[54] The different experimentally reported isotherms, however, differ drastically. Although the isotherm reported by Schoenecker et al.[54] is in excellent agreement with the one measured by Yang et al.,[55] the loading of Grant Glover et al.[56] is significantly lower than that of Schoenecker et al.[54] One of the possible explanations for this discrepancy is the reported Langmuir surface areas of different samples, which vary from 1400 to 2000 m^2/g. Additionally, the materials can be possibly decomposed in the presence of water vapors.[54] These experimental differences make it difficult to properly validate the different models at higher-pressure.

Figures 5 and 6 show the comparison between the computed and experimental adsorption properties in Cu-BTC. Similar to the case of Mg-MOF-74, the results show that the refined potentials provide significant improvements compared to the ones without adjustments. TIP5P-Ew models also show an unusual pronounced plateau in uptake before condensation, which is not observed from the experimental data. As of the high-pressure loading, the uncertainties and inconsistencies in the experimental measurements make it difficult for a fair comparison.

At this point, it is intriguing to compare our refined potential with the one proposed by Zang et al.[57] In their study on the water adsorption in Cu-BTC, DFT calculations are used to obtain an empirical correction function added to commonly used force fields based on about a 1000 single-point calculations, which is denoted as OCuFF force field. As shown in Figures 5 and 6, OCuFF still yields a poor estimate in adsorption properties, in particular at low pressure region, therefore, a further correction was required (i.e., OCuFF-modified). Both of the approaches proposed by Zang et al.[57] and our method aim at correcting H_2O-metal interaction directly based on DFT calculations. However, the approach used in this study is relatively straightforward and requires much less computation cost. It should be noted that some other methodologies have also been introduced to derive force fields in details from quantum calculations to model H_2O adsorptions in Mg-MOF-74.[10,58] Similarly, the computational cost of these methods is expected to be more expensive than the method adopted in this work.

Analysis of adsorbed configurations at higher-pressure region

To provide deeper insights into the difference in the uptake of these three H_2O models at the higher-pressure region, we plot in Figure 7 the density maps of the oxygen atoms of H_2O molecules in Mg-MOF-74 and the corresponding density profiles quantitatively shown in Figure 8. This analysis uses the force fields without refinements as no notable differences in uptake at 2.2 kPa between force fields with and without refinement are observed.

Figure 7 shows that all three models predict the water molecules to be preferentially adsorbed to the Mg atoms, and a secondary adsorption sites located on the top of the benzene rings of the Mg-MOF-74 linkers. These preferential binding sites can be also observed from the peaks of $g_o(\theta)$ in Figure 8a. Surprisingly, Figure 7 also shows that the water structure computed by SPC/E and TIP4P-Ew has an inner square-like ring while TIP5P-Ew has a looser and uniform distribution in the center of the pore. These observations are also reflected on the density profiles as shown in Figures 8b, c. Figure 8b illustrates that, compared to the TIP5P-Ew model, the SPC/E and TIP4P-Ew models have higher probabilities at $r = \sim 0.2$ nm, indicating the occurrence of an inner ring. Figure 8c shows that, along the *z* axis, the TIP5P-Ew model gives a lower and uniform density distribution. These observations suggest that the SPC/E and TIP4P-Ew models predict a more structured and organized water network than the one by TIP5P-Ew model, which results in the differences of the loadings at higher-pressure region.

Furthermore, the orientational order parameters of H_2O with respect to the pore surface and pore axis are shown in Figure 9. It is interesting to see that both the SPC/E and

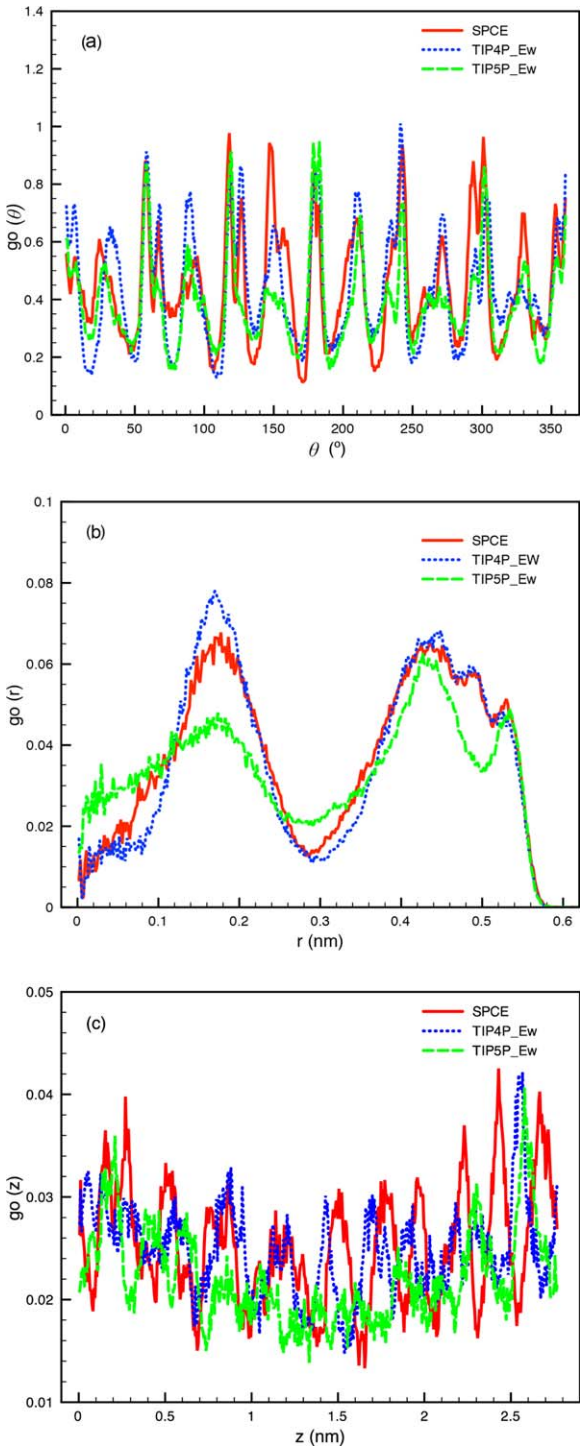

Figure 8. Probability densities of the oxygen atoms of H_2O molecules as a function of (a) angle, (b) radius, and (c) distance along the *z* axis at 2.2 kPa and 298 K.

The definition of adopted coordinates can be found in Supporting Information Figure S1b. [Color figure can be viewed in the online issue, which is available at wileyonlinelibrary.com.]

TIP4P-Ew models predict more ordered configurations for those water molecules adsorbed at the secondary binding sites, that is, benzene ring at $r = \sim 0.43$ nm, than those computed by TIP5P-Ew. The less ordered configurations with TIP5P-Ew model may lead to a lower H_2O adsorption density in the center of the pore.

Conclusions

Water adsorption properties inside different classes of materials including zeolites, ZIFs, and MOFs are investigated using different water models. The predicted properties for a special set of MOFs with so-called open-metal sites, compare to others, are found to be extremely sensitive to the details of the water models. The conventional force fields are shown to largely underestimate the adsorption energies in these materials. Among several water models, this work demonstrates that more than 3 sites models are necessary to represent the binding geometry in these MOFs with open metal sites; particularly TIP5P-Ew model gives a consistent and better representation of binding configuration.

To provide accurate prediction in water adsorption, in this work, we used a simple but effective strategy to correct H_2O-Metal repulsion distance by optimizing O(H_2O)-metal σ parameter to best reproduce DFT-binding energies. The corresponding simulated isotherms at low-pressure region are in much better agreement with experimentally reported ones compared to the commonly used force field. Surprisingly,

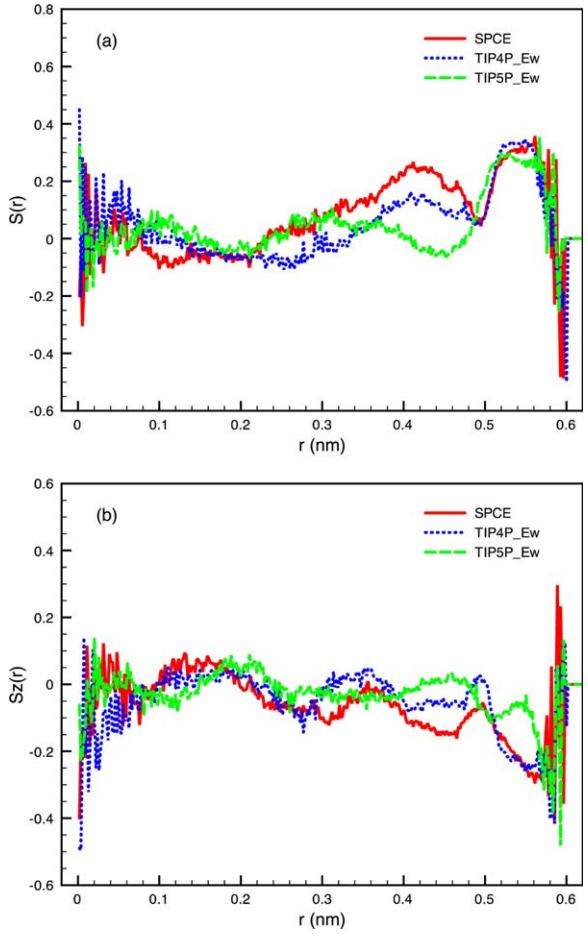

Figure 9. Distributions of the orientational order parameters as a function of distance with respect to (a) Mg-MOF-74 surface, (b) Mg-MOF-74 pore axis at 2.2 kPa and 298 K.

[Color figure can be viewed in the online issue, which is available at wileyonlinelibrary.com.]

the TIP5P-Ew model shows a much more pronounced plateau before the occurrence of capillary condensation, which is not observed in the experimental data.

Moreover, the structure of adsorbed H_2O molecules at high-pressure region, that is, water network, in Mg-MOF-74 is quantitatively studied by examining orientational order parameters and probability densities. A double-ring water structure along the *z*-direction is observed for SPC/E and TIP4P-Ew models while TIP5P-Ew shows a relatively disordered structure in the channel. The relatively disordered structure is attributed to the water configurations adsorbed on the benzene rings.

Acknowledgments

XP was supported by the Open Project of State Key Laboratory of Chemical Engineering (SKL-Che-12C01). XP and WZS were supported by the China Scholarship Council. LCL and BS were supported as part of the Center for Gas Separations Relevant to Clean Energy Technologies, an Energy Frontier Research Center funded by the U.S. Department of Energy, Office of Science, Office of Basic Energy Sciences under Award Number DE-SC0001015.

Literature Cited

1. Smit B, Reimer JA, Oldenburg CM, Bourg IC. Introduction to Carbon Capture and Sequestration. London: Imperial College Press, 2014.
2. Peng X, Wang W, Xue R, Shen Z. Adsorption separation of CH_4/CO_2 on mesocarbon microbeads: experiment and modeling. *AIChE J*. 2006;52:994–1003.
3. Lin L-C, Berger AH, Martin RL, Kim J, Joseph A, Jariwala K, Rycroft CH, Bhown AS, Michael W. In silico screening of carbon-capture materials. *Nat Mater*. 2012;11:633–641.
4. Banerjee R, Phan A, Wang B, Knobler C, Furukawa H, O'Keeffe M, Yaghi OM. High-throughput synthesis of zeolitic imidazolate frameworks and application to CO_2 capture. *Science*. 2008;319:939–943.
5. Park KS, Ni Z, Côté AP, Choi JY, Huang R, Uribe-Romo FJ, Chae HK, O'Keeffe M, Yaghi OM. Exceptional chemical and thermal stability of zeolitic imidazolate frameworks. *Proc Natl Acad Sci USA*. 2006;103:10186–10191.
6. Morris W, Leung B, Furukawa H, Yaghi OK, He N, Hayashi H, Houndonougbo Y, Asta M, Laird BB, Yaghi OM. A combined experimental-computational investigation of carbon dioxide capture in a series of isoreticular zeolitic imidazolate frameworks. *J Am Chem Soc*. 2010;132:11006–11008.
7. Chui SS-Y, Lo SM-F, Charmant JPH, Orpen AG, Williams ID. A chemically functionalizable nanoporous material $[Cu_3(TMA)_2(H_2O)_3]n$. *Science*. 1999;283:1148–1150.
8. Eddaoudi M, Kim J, Rosi N, Vodak D, Wachter J, O'Keeffe M, Yaghi OM. Systematic design of pore size and functionality in isoreticular MOFs and Their application in methane storage. *Science*. 2002;295:469–472.
9. Yaghi OM, O'Keeffe M, Ockwig NW, Chae HK, Eddaoudi M, Kim J. Reticular synthesis and the design of new materials. *Nature*. 2003;423:705–714.
10. Lin L-C, Lee K, Gagliardi L, Neaton JB, Smit B. Force-field development from electronic structure calculations with periodic boundary conditions: applications to gaseous adsorption and transport in metal–organic frameworks. *J Chem Theory Comput*. 2014;10:1477–1488.
11. Yazaydın AÖ, Benin AI, Faheem SA, Jakubczak P, Low JJ, Willis RR, Snurr RQ. Enhanced CO_2 adsorption in metal-organic frameworks via occupation of open-metal sites by coordinated water molecules. *Chem Mater*. 2009;21:1425–1430.
12. Greathouse JA, Allendorf MD. The interaction of water with MOF-5 simulated by molecular dynamics. *J Am Chem Soc*. 2006;128:10678–10679.
13. Koga K, Gao GT, Tanaka H, Zeng XC. Formation of ordered ice nanotubes inside carbon nanotubes. *Nature*. 2001;412:802–805.
14. Mashl RJ, Joseph S, Aluru NR, Jakobsson E. Anomalously immobilized water: a new water phase induced by confinement in nanotubes. *Nano Lett*. 2003;3:589–592.
15. Hummer G, Rasaiah JC, Noworyta JP. Water conduction through the hydrophobic channel of a carbon nanotube. *Nature*. 2001;414:188–190.
16. Introduction to water models. Available at http://www1.lsbu.ac.uk/water/water_models.html.
17. Frenkel D, Smit B. Understanding Molecular Simulation: From Algorithms to Applications, 2nd ed. New York: Academic Press, 2002.
18. Castillo JM, Dubbeldam D, Vlugt TJH, Smit B, Calero S. Evaluation of various water models for simulation of adsorption in hydrophobic zeolites. *Mol Simul*. 2009;35:1067–1076.
19. Horn HW, Swope WC, Pitera JW. Characterization of the TIP4P-Ew water model: vapor pressure and boiling point. *J Chem Phys*. 2005;123:194504–194512.
20. Jorgensen WL, Chandrasekhar J, Madura JD, Impey RW, Klein ML. Comparison of simple potential functions for simulating liquid water. *J Chem Phys*. 1983;79:926–935.
21. Mahoney MW, Jorgensen WL. A five-site model for liquid water and the reproduction of the density anomaly by rigid, nonpolarizable potential functions. *J Chem Phys*. 2000;112:8910–8922.
22. Mao Y. Prediction of the Temperature-dependent thermal conductivity and shear viscosity for rigid water models. *J Nanotechnol Eng Med*. 2013;3:031010–031017.
23. Mark P, Nilsson L. Structure and dynamics of the TIP3P, SPC, and SPC/E water models at 298 K. *J Phys Chem A*. 2001;105:9954–9960.
24. Nada H, van der Eerden JPJM. An intermolecular potential model for the simulation of ice and water near the melting point: a six-site model of H_2O. *J Chem Phys*. 2003;118:7401.
25. Rick SW. A reoptimization of the five-site water potential (TIP5P) for use with Ewald sums. *J Chem Phys*. 2004;120:6085–6093.
26. Vega C, Sanz E, Abascal JLF. The melting temperature of the most common models of water. *J Chem Phys*. 2005;122:114507–114509.
27. Rappe AK, Casewit CJ, Colwell KS, Goddard WA III, Skiff WM. UFF, a full periodic table force field for molecular mechanics and molecular dynamics simulations. *J Am Chem Soc*. 1992;114:10024–10035.
28. García-Sańchez A, Ania CO, Parra JB, Dubbeldam D, Vlugt TJH, Krishna R, Calero S. Transferable force field for carbon dioxide adsorption in zeolites. *J Phys Chem C*. 2009;113:8814–8820.
29. Liu B, Smit B. Comparative molecular simulation study of CO_2/N_2 and CH_4/N_2 separation in zeolites and metal-organic frameworks. *Langmuir*. 2009;25:5918–5926.
30. Peng X, Cao D. Computational Screening of porous carbons, zeolites, and metal organic frameworks for desulfurization and decarburization of biogas, natural gas, and flue gas. *AIChE J*. 2013;59:2928–2942.
31. Peng X, Cheng X, Cao D. Computer Simulations for the adsorption and separation of CO_2/CH_4/H_2/N_2 gases by UMCM-1 and UMCM-2 metal organic frameworks. *J Mater Chem*. 2011;21:11259–11270.
32. Dzubak AL, Lin L-C, Kim J, Swisher JA, Poloni R, Maximoff SN, Smit B, Gagliardi L. Ab initio carbon capture in open-site metal-organic frameworks. *Nat Chem*. 2012;4:810–816.
33. Bruinsma RF, De Gennes PG, Freund JB, Levine D. A route to high surface area, porosity and inclusion of large molecules in crystals. *Nature*. 2004;427:523–527.
34. Millward AR, Yaghi OM. Metal-organic frameworks with exceptionally high capacity for storage of carbon dioxide at room temperature. *J Am Chem Soc*. 2005;127:17998–17999.
35. Dietzel PDC, Morita Y, Blom R, Fjellvåg H. An in situ high-temperature single-crystal investigation of a dehydrated metal-organic framework compound and field-induced magnetization of one-dimensional metal-oxygen chains. *Angew Chem Int Ed*. 2005;44:6354–6358.
36. Dietzel PDC, Panella B, Hirscher M, Blom R, Fjellvåg H. Hydrogen adsorption in a nickel based coordination polymer with open metal sites in the cylindrical cavities of the desolvated framework. *Chem Commun*. 2006;1:959–961.
37. Yazaydin AO, Snurr RQ, Park T-H, Koh K, Liu J, Levan MD, Benin AI, Jakubczak P, Lanuza M, Galloway DB, Low JJ, Willis RR. Screening of metal-organic frameworks for carbon dioxide capture from flue gas using a combined experimental and modeling approach. *J Am Chem Soc*. 2009;131:18198–18199.
38. Barthelet K, Marrot J, Riou D, Férey G. A breathing hybrid organic-inorganic solid with very large pores and high magnetic characteristics. *Angew Chem Int Ed*. 2002;41:281–284.

39. Rosenbach N, Jobic H, Ghoufi A, Salles F, Maurin G, Bourrelly S, Llewellyn PL, Devic T, Serre C, Férey G. Quasi-elastic neutron scattering and molecular dynamics study of methane diffusion in metal organic frameworks MIL-47(V) and MIL-53(Cr). *Angew Chem Int Ed*. 2008;47:6611–6615.
40. Koh K, Wong-Foy AG, Matzger AJ. A crystalline mesoporous coordination copolymer with high microporosity. *Angew Chem Int Ed*. 2008;47:677–680.
41. Deng H, Grunder S, Cordova KE, Valente C, Furukawa H, Hmadeh M, Gándara F, Whalley AC, Liu Z, Asahina S, Kazumori H, O'Keeffe M, Terasaki O, Stoddart JF, Yaghi OM. Large-Pore apertures in a series of metal-organic frameworks. *Science*. 2012;336: 1018–1023.
42. Caskey SR, Wong-Foy AG, Matzger AJ. Dramatic Tuning of carbon dioxide uptake via metal substitution in a coordination polymer with cylindrical pores. *J Am Chem Soc*. 2008;130:10870–10871.
43. Dietzel PDC, Besikiotis V, Blom R. Application of metal–organic frameworks with coordinatively unsaturated metal sites in storage and separation of methane and carbon dioxide. *J Mater Chem*. 2009; 19:7362.
44. Dietzel PDC, Blom R, Fjellvåg H. Base-Induced formation of two magnesium metal-organic framework compounds with a bifunctional tetratopic ligand. *Eur J Inorg Chem*. 2008;2008:3624–3632.
45. Rosi NL, Kim J, Eddaoudi M, Chen B, Keeffe MO, Yaghi OM. Rod packings and metal - organic Frameworks constructed from rod-shaped secondary building units. *J Am Chem Soc*. 2005;127:1504–1518.
46. Rowsell JLC, Yaghi OM. Effects of functionalization, catenation, and variation of the metal oxide and organic linking units on the low-pressure hydrogen adsorption properties of metal-organic frameworks. *J Am Chem Soc*. 2006;128:1304–1315.
47. Lin L-C, Kim J, Kong X, Scott E, McDonald TM, Long JR, Reimer JA, Smit B. Understanding CO_2 dynamics in metal-organic frameworks with open metal sites. *Angew Chem Int Ed*. 2013;52:4410–4413.
48. Yang Q, Ma L, Zhong C, An X, Liu D. Enhancement of CO_2/N_2 mixture separation using the thermodynamic stepped behavior of adsorption in metal−organic frameworks. *J Phys Chem C*. 2011;115: 2790–2797.
49. Coasne B, Fourkas JT, Normale E. Structure and dynamics of benzene confined in silica nanopores. *J Phys Chem C*. 2011;115:15471–15479.
50. Lee K, Murray ÉD, Kong L, Lundqvist BI, Langreth DC. Higher-accuracy Van Der Waals density functional. *Phys Rev B*. 2010;82: 081101.
51. Watanabe T, Sholl DS. Molecular chemisorption on open metal sites in Cu(3)(benzenetricarboxylate)(2): a spatially periodic density functional theory study. *J Chem Phys*. 2010;133:094509.
52. Grajciar L, Bludsky´ O, Nachtigall P. Water Adsorption on coordinatively unsaturated sites in CuBTC MOF. *J Phys Chem Lett*. 2010;1: 3354–3359.
53. Sun WZ, Lin L-C, Peng X, Smit B. Computational screening of porous metal-organic frameworks and zeolites for the removal of SO_2 and NO_x from flue gases. *AIChE J*. 2014;60:2314–2323.
54. Schoenecker PM, Carson CG, Jasuja H, Flemming CJJ, Walton KS. Effect of water adsorption on retention of structure and surface area of metal–organic frameworks. *Ind Eng Chem Res*. 2012;51:6513–6519.
55. Yang D-A, Cho H-Y, Kim J, Yang S-T, Ahn W-S. CO_2 capture and conversion using Mg-MOF-74 prepared by a sonochemical method. *Energy Environ Sci*. 2012;5:6465–6473.
56. Grant Glover T, Peterson GW, Schindler BJ, Britt D, Yaghi O. MOF-74 building unit has a direct impact on toxic gas adsorption. *Chem Eng Sci*. 2011;66:163–170.
57. Zang J, Nair S, Sholl DS. Prediction of water adsorption in copper-based metal–organic frameworks using force fields derived from dispersion-corrected DFT calculations. *J Phys Chem C*. 2013;117: 7519–7525.
58. Rudenko AN, Bendt S, Keil FJ. Multiscale modeling of water in Mg-MOF-74: from electronic structure calculations to adsorption isotherms. *J Phys Chem C*. 2014;118:16218–16227.

Manuscript received July 27, 2014, and revision received Dec. 3, 2014.